Since January 2020 Elsevier has created a COVID-19 resource centre with free information in English and Mandarin on the novel coronavirus COVID-19. The COVID-19 resource centre is hosted on Elsevier Connect, the company's public news and information website.

Journal of Environmental Management 291 (2021) 112676

Contents lists available at ScienceDirect

Journal of Environmental Management

journal homepage: www.elsevier.com/locate/jenvman

Research article

Quantitative estimation of meteorological impacts and the COVID-19 lockdown reductions on NO_2 and $PM_{2.5}$ over the Beijing area using Generalized Additive Models (GAM)

Jinxi Hua [a], Yuanxun Zhang [a,b,*], Benjamin de Foy [c], Jing Shang [d], James J. Schauer [e], Xiaodong Mei [a], Ishaq Dimeji Sulaymon [a], Tingting Han [d]

[a] College of Resources and Environment, University of Chinese Academy of Sciences, Beijing, China
[b] CAS Center for Excellence in Regional Atmospheric Environment, Chinese Academy of Sciences, Xiamen, China
[c] Department of Earth and Atmospheric Sciences, Saint Louis University, St. Louis, MO, USA
[d] Institute of Urban Meteorology, China Meteorological Administration, Beijing, China
[e] Wisconsin State Laboratory of Hygiene, University of Wisconsin-Madison, Madison, WI, USA

ARTICLE INFO

Keywords:
meteorology
COVID-19 lockdown
GAM analysis
Spatial patterns
Diurnal profiles

ABSTRACT

Unprecedented travel restrictions due to the COVID-19 pandemic caused remarkable reductions in anthropogenic emissions, however, the Beijing area still experienced extreme haze pollution even under the strict COVID-19 controls. Generalized Additive Models (GAM) were developed with respect to inter-annual variations, seasonal cycles, holiday effects, diurnal profile, and the non-linear influences of meteorological factors to quantitatively differentiate the lockdown effects and meteorology impacts on concentrations of nitrogen dioxide (NO_2) and fine particulate matters ($PM_{2.5}$) at 34 sites in the Beijing area. The results revealed that lockdown measures caused large reductions while meteorology offset a large fraction of the decrease in surface concentrations. GAM estimates showed that in February, the control measures led to average NO_2 reductions of 19 μg/m^3 and average $PM_{2.5}$ reductions of 12 μg/m^3. At the same time, meteorology was estimated to contribute about 12 μg/m^3 increase in NO_2, thereby offsetting most of the reductions as well as an increase of 30 μg/m^3 in $PM_{2.5}$, thereby resulting in concentrations higher than the average $PM_{2.5}$ concentrations during the lockdown. At the beginning of the lockdown period, the boundary layer height was the dominant factor contributing to a 17% increase in NO_2 while humid condition was the dominant factor for $PM_{2.5}$ concentrations leading to an increase of 65% relative to the baseline level. Estimated NO_2 emissions declined by 42% at the start of the lockdown, after which the emissions gradually increased with the increase of traffic volumes. The diurnal patterns from the models showed that the peak of vehicular traffic occurred from about 12pm to 5pm daily during the strictest control periods. This study provides insights for quantifying the changes in air quality due to the lockdowns by accounting for meteorological variability and providing a reference in evaluating the effectiveness of control measures, thereby contributing to air quality mitigation policies.

1. Introduction

The coronavirus 2019 (COVID-19) pandemic has been an immense threat to public health security, and corresponding lockdown measures have caused worldwide economic recessions (Wang et al., 2020c). The World Health Organization reported that, as of December 4, 2020, the cumulative number of infections and deaths of COVID-19 cases has exceeded 71.5 million and 1.6 million, respectively (World Health Organization, 2020). To control the spread of COVID-19 from person to person, the Chinese authorities implemented a city-wide lockdown of Wuhan on January 23, 2020, and other cities also took a series of dramatic actions within a few days (Tian et al., 2020; Bao et al., 2020; Sulaymon et al., 2021). Beijing initiated first-level emergency response on January 24, 2020 which lasted until April 30, 2020 (Xinhua Net, 2020). The strict regulations at the beginning of the pandemic were taken to minimize human outdoor activities, e.g. public transportations outages, restaurants closures, and construction and non-essential factories suspensions (Bao and Zhang, 2020).

* Corresponding author. CAS Center for Excellence in Regional Atmospheric Environment, Chinese Academy of Sciences, Xiamen, China.
E-mail address: yxzhang@ucas.ac.cn (Y. Zhang).

https://doi.org/10.1016/j.jenvman.2021.112676
Received 9 January 2021; Received in revised form 4 March 2021; Accepted 28 March 2021
Available online 4 May 2021

The COVID-19 lockdown resulted in dramatic drops in traffic and industrial emissions, and demonstrated significant improvements to air quality on local and regional scales (Fan et al., 2020; Chu et al., 2020; Venter et al., 2020; Diamond et al., 2020; Silver et al., 2020). According to TROPOMI instrument observations in Chinese cities, the nitrogen dioxide (NO_2) vertical column densities dropped by about 40% in January–April 2020 compared with the same period in 2019 (Bauwens et al., 2020). The decreased nitrogen oxides (NO_x) levels during the lockdown in eastern China, approximately 70–80%, can be attributed to the reduced transportation emissions and 20–25% can be attributed to the reduced industrial emissions (Huang et al., 2020). During the control period, there were smaller reductions in $PM_{2.5}$ compared to NO_2 as $PM_{2.5}$ is primarily due to household and industrial coal-burning emissions, and these activities were relatively less impacted by the lockdown (Diamond and Wood, 2020; Silver et al., 2020). The primary sources of $PM_{2.5}$ reduced by 30–50% and the secondary aerosol species reduced by 12–15% in 2020 based on a six-year chemical species analysis during Chinese New Year (Sun et al., 2020).

Meteorology plays an important role in the formation, transportation, and diffusion processes of air pollutants, especially during the winter (Wang et al., 2016; Wang et al., 2017; Griffith et al., 2020). An unexpected haze episode was observed with high-level $PM_{2.5}$ concentrations during the first week of the COVID-19 lockdown in the Beijing area (Huang et al., 2020; Chang et al., 2020; Wang et al., 2020b; Cui et al., 2020). The extreme air pollution was mainly caused by unfavorable meteorological conditions, specifically, high relative humidity promoted the rapid growth of secondary aerosol particles and stagnant airflow contributed to the accumulation of pollutant (Sun et al., 2020; Chang et al., 2020; Le et al., 2020).

Due to the unexpected haze events during the pandemic, meteorological impacts are crucial to evaluating the effects of the COVID-19 lockdown. The widespread use of the concentration difference between the lockdown in 2020 and the same period in previous years to evaluate the impacts of COVID-19 control measures on air quality could be biased (Fan et al., 2020; Otmani et al., 2020). Multiple linear regressions have been widely used to account for meteorological impacts and thus quantify the COVID-19 lockdown impacts more accurately (Venter et al., 2020; Diamond and Wood, 2020; Liu et al., 2020). However, regression methods often assume that there is a linear relationship between meteorology and pollutant concentration. Machine learning methods that normalize the influence of weather have high predictive performance, but are usually black box models that lack interpretability (Petetin et al., 2020; Grange et al., 2019). Clarifying the impact of human activities and meteorological factors on air quality during major events is crucial to the formulation of pollution control policies during major events and the long-term air pollution control policies of Beijing. Generalized Additive Models (GAM) can balance the fitting performance and have high interpretability, it is a useful tool to estimate the air quality responses to human activities and meteorology (Zhou et al., 2012; Ma et al., 2020). Ma et al. (2020) used GAM to estimate the effects of meteorology on tropospheric ozone in Lanzhou, China, and found that the method gave improved estimates with respect to the temporal variations. In contrast to parametric models, GAM does not need prior knowledge and can determine relationships in the measurements using data-driven analysis (Zhou et al., 2012). The GAM method captured the variation of $PM_{2.5}$ better than linear models for the calibration of particulate low-cost sensors by meteorology adjustment (Hua et al., 2021a).

In this study, a GAM was developed to quantify the meteorology and lockdown effects with respect to multi-temporal patterns and nonlinear impacts from meteorological parameters using hourly $PM_{2.5}$ and NO_2 measurements from January to June 2015 to 2020. The whole study period was divided into six groups: the pre-lockdown period (the days before January 23, 2020) and roughly every month from February to June in 2020. Inter-annual trends, seasonality, and holiday effects were considered separate from the influence of the COVID-19 lockdown. Boundary layer heights and wind components were used to characterize the vertical mixing ratio and horizontal dispersion. The spatial patterns of time-varying lockdown effects and diurnal profiles were analyzed according to various land-use types.

2. Materials and methods

2.1. Ground-based air quality measurements and traffic data

The hourly $PM_{2.5}$ and NO_2 measurements from January to June in 2015–2019 were obtained from the Beijing Municipal Environmental Monitoring Center (http://www.bjmemc.com.cn/). The network includes 34 monitoring sites (Fig. S1) in Beijing. For each site, the data availability was more than 90% over the entire period, which means there were more than 23,500 data points out of 26,112 h (Table S1). The 34 air quality monitoring sites were classified into three groups based on urbanization levels (Hua et al., 2021b). The sites within the Fifth Ring Road were defined as downtown, and had the highest level of urbanization. The sites between the Fifth Ring Road and the Sixth Ring Road were defined as suburban, while the remaining sites with the lowest level of urbanization and sparse population density were categorized as the rural areas.

The weekly congestion levels at Beijing were obtained from public real-time traffic reports (https://www.tomtom.com/en_gb/traffic-index/beijing-traffic/) which are calculated from hourly data. In this study, the congestion level differences in 2020 relative to 2019 were used to represent changes in traffic volumes in 2020.

2.2. Meteorological observations

Meteorological observations and simulations from three sources were used as potential inputs for the analysis, and the model selected the variables that gave the best fit as described in Section 2.3. The meteorological data sources were the fifth-generation atmospheric reanalysis dataset from the European Centre for Medium-Range Weather Forecasts (ERA5, https://cds.climate.copernicus.eu/); the observations from Beijing Capital International Airport (40.08°N, 116.585°E) (Figure S1) from the Integrated Surface Database of the National Oceanic and Atmospheric Administration (NOAA) (ISD, https://www.ncdc.noaa.gov/isd/data-access); and 14 meteorological stations (Figure S1) operated by the Beijing Meteorological Bureau (BJ). The meteorological variables from ERA5 included boundary layer height (BLH), zonal velocity (U), meridional velocity (V), relative humidity (RH), air temperature at 2 m above the surface (T2M), dew point temperature at 2 m above the surface (D2M), and surface pressure (SP). The original grids with 0.25° resolution were linearly interpolated to 0.01*0.01° and a time series for each station can be extracted from the nearest grid. The hourly surface meteorological parameters obtained from ISD and BJ, included U, V, RH, T2M, D2M, SP and U, V, RH, T2M, SP, and precipitation (P). The observation data from 14 stations of Beijing Meteorological Bureau were matched with the nearest air quality station in order to obtain local meteorological conditions.

The hourly boundary layer heights were converted to rolling averages from one to 3 h to perform optimal variable selections. The hourly precipitation was converted to 24-hr cumulative precipitation. Hourly RH, T2M, D2M, and SP were calculated as 24-hr rolling averages to use as inputs for the models. The time of all data points was unified to China Standard Time (CST, UTC + 8).

2.3. Generalized additive model (GAM) analysis

A GAM including multi-temporal variations and meteorological parameters was used to quantify the impact from each factor on $PM_{2.5}$ and NO_2 concentrations. In this study, the temporal variables include inter-annual trends, seasonal cycles, day of the week patterns, different lockdown periods and diurnal variations (Table 1). The meteorological

Table 1
The type of functions to characterize the relationships between predictors and pollutant concentrations, and the definition of each factor including in GAM analysis. Categorial functions represent the variables are dummy vectors with values of 1 during the time interval otherwise the values are 0. Variables in brackets indicate the list of meteorological candidates. More details can be seen in the main text.

Predictors	Functions	Factors
Interannual	Linear	Time series of days since January 1, 2015.
Monthly	Smooth	January to June.
Weekly	Category	Weekdays, Weekends, Holidays in the heating season, Tomb Sweeping Day, Holidays in the non-heating season.
Lockdown	Category	Pre-lockdown, every month from February to June in 2020.
Diurnal	Category	Three factors (Pre-lockdown, lockdown, Post-lockdown) for each hour of the day.
Meteorology	Smooth	Boundary layer height, winds, (relative humidity, dew point temperature, air temperature, surface pressure and precipitation).

factors included BLH, U, V, RH, T2M, D2M, SP and P (Table 1). The types of functions for temporal variables characterized the change of emissions and the types of functions for meteorology characterized the relationship between meteorology and air quality. The selections of function type for interannual, seasonal, weekly, diurnal and meteorology were referenced from some previous studies (Zhou et al., 2012; de Foy, 2018; de Foy and Schauer, 2019) and were also tested for the Beijing area in our recent study (Hua et al., 2021b). The interannual variable used a linear trend to characterize the decline in air pollutant concentrations. This was mainly influenced by the long-term control policies. The seasonal variation used a non-linear function which was mainly related to the variation of meteorology and the emissions for heating during the winter. The category functions for weekly and diurnal were mainly related to human behaviors, such as most people work on weekdays and have a rest on weekends and holidays, the diurnal variation related to traffic volumes during a day. The function type of lockdown variable was applied in this study which was based on the consideration of the sudden implementation of strict control measures at the beginning of COVID-19 pandemic and the economic recovery level was different at different stages. The relationship between air quality and predictors as preliminary definitions (Table 1) can be obtained from GAM analysis (Fig. S2). The models are described by Eq (1):

$$\log(Conc_s + offset) = \alpha_{yr} t_{yr} + s_1(t_{month}) + \sum_{n=1}^{5} \alpha_{wkd_n} t_{wkd_n} + \sum_{k=1}^{6} \alpha_{ld_k} t_{ld_k} + \sum_{i=1}^{3} \times \sum_{h=1}^{24} \alpha_{hr_{i,h}} t_{hr_{i,h}} + s_2(BLH) + s_3(U,V) + s_4(Optimized\ Input) + \alpha_{baseline} + \in \quad (1)$$

$Conc_s$ are the time series of $PM_{2.5}$ or NO_2 concentrations at s site from January to June during 2015–2020. In order to approximate normal distribution, the hourly measurements were logarithm transformed and added offset of 3 μg/m^3 for $PM_{2.5}$ and of 16 μg/m^3 for NO_2, respectively. The offset value of $PM_{2.5}$ and NO_2 were based on preliminary tests. α are the regression coefficients and $\alpha_{baseline}$ is derived from model and used to represent the average concentrations after accounting for the impacts from all the factors in the model. $s()$ are the smooth functions used to characterize the non-linear impacts of seasonal variations and meteorological parameters on air quality.

t denotes temporal term, including signals for yearly, monthly, day of the week, the lockdown and each hour of the day. t_{yr} is the continuous number of days labeled from January 1, 2015 to June 30, 2020. t_{month} represents the month from January to June in each year. t_{wk} denotes the dummy variables categorized to the weekdays (n = 1), weekends (n = 2), and holidays (n values are from 3 to 5). The holidays were classified by three groups: n = 3 means the holidays during the heating season (including New Year's Day, Chinese New Year, and Lantern Festival), n = 4 means Tomb Sweeping Day, and n = 5 means the holidays during the non-heating season (Labor Day, Dragon Boats Festival). The detailed information about dates of each holiday as shown in Section 1 in Supplementary Materials and also provided in Table S2.

To identify the impacts of the COVID-19 control measures on air quality over time, t_{ld} were separated into 6 categories: the pre-lockdown period, and then roughly every month from February to June during 2020. GAM analysis for hourly $PM_{2.5}$ and NO_2 measurements used $t_{hr_{i,h}}$ for each hour of the day for different lockdown periods to represent diurnal variations. h is each hour of the day. i represents separated diurnal factors for the pre-lockdown period (Pre-LD: the data points before January 23, 2020), during the lockdown period (LD: the data points from January 23 to March 31, 2020), and post-lockdown period (Post-LD: the data points from April 1 to June 30, 2020), for a total of 3 sets of 24 factors. Overall, the whole period was grouped into 3 categories for diurnal variations and 6 categories for lockdown effects, detailed information about lockdown definitions as shown in Section 1 in Supplementary Materials and also provided in Table S3.

BLH and wind components were included in the models to characterize the impacts of vertical and horizontal diffusion on air quality. BLH was selected as the one with the highest correlation coefficients squared (r^2) from preceding 1-hr to 3-hr rolling means. Wind components were selected as the variables with the highest fitting performance from ERA5, ISD, and BJ data sources based on iteratively runs. *Optimized input* was selected using a stepwise forward process from meteorological candidates as described in (de Foy et al., 2015; de Foy et al., 2019). The model started with only one candidate variable and gradually added the one with the greatest contribution to r^2 until an increase in r^2 of at least 0.005. The meteorological candidates include 24-hr cumulative of P and 24-hr running average of RH, T2M, D2M, and SP from ERA5, ISD, and BJ, respectively. This was done to cancel out the diurnal variability of climatology such as the BLH rise, which began in the morning and reached a maximum in the afternoon (Chu et al., 2019; Mehta et al., 2017), so that the diurnal profiles of GAM results would be closer to the emissions changes (de Foy and Schauer, 2019; Wang et al., 2020a). Meteorological parameters were linearly scaled to approximate a normal distribution of zero mean and unit standard deviation to reduce the effects of extreme observations, hence, their impacts on average baseline concentrations were close to 0.

Except for $\alpha_{baseline}$, a weighting factor of 1 was used as a penalty term forcing coefficients to get minimum values (de Foy et al., 2015b; de Foy et al., 2020). Iteratively Reweighted Least Squares (IRLS) method was used to remove the outliers: the data points with a residual greater than four times the standard deviation of all the residuals were excluded from the analysis. Block-bootstrapping with 7-day chunks was used to estimate the uncertainty from GAM analysis (de Foy et al., 2020; de Foy, 2018; de Foy et al., 2016). The models ran 100 times with randomly resampled same size data points from the original dataset and the standard deviation of regression coefficients were obtained from 100 realizations. This method avoids the estimation bias caused by extreme situations, such as the occasional appearance of a haze episode.

The results can be interpreted in three ways (de Foy and Schauer, 2019). The time vectors (such as t_{wd}, t_{ld}, t_{hr}) with values of 1 represent during the time interval and values of 0 represent the other time intervals, namely baseline conditions. Therefore, the first way to interpret the results is the Percent Relative Effect of each factor on concentrations (p) using Eq (2) which represent the percentage change of concentrations relative to baseline. The second way is the difference in concentrations relative to the baseline level (ΔC) based on Eq (3), it indicates how much the concentrations deviated from the expected values. The third way is the adjusted concentrations (C_{adj}) with respect to

meteorology and the temporal influences, the calculation method is Eq (4).

$$p = (e^{\alpha} - 1) \times 100\% \quad (2)$$

$$\Delta C = (e^{\alpha} - 1) \times e^{\alpha_{baseline}} \quad (3)$$

$$C_{adj} = e^{\alpha} e^{\alpha_{baseline}} - offset \quad (4)$$

3. Results and discussions

3.1. Characteristics of air quality measurements and meteorological observations

3.1.1. Seasonal variations

The time series of the 10 days rolling average concentrations of air quality measurements in each year at GC are shown in Fig. 1. The site is located in the western suburban area and surrounded by mixed commercial and residential areas, which are strongly influenced by human activities. The annual time series shows high variability of concentrations from year to year due to changing emissions and meteorological impacts. The differences in concentration between 2020 and the previous 5 years (2015–2019) is therefore not a reliable estimate of the lockdown effect, as shown in Figs. 2a and 2b. An average decline of 19 μg/m^3 for NO_2 (Figs. 2a) and 17 μg/m^3 for $PM_{2.5}$ (Fig. 2b) was observed between the 2015–2019 average and 2020, reflecting the effects of air clean control policies in recent years and the influences of the COVID-19 shut down measures in 2020 (Venter et al., 2020; de Foy et al., 2016; Baumgartner et al., 2019; Shang et al., 2018; Tian et al., 2019; Zhang et al., 2016a). It exhibited high seasonal variability with the maximum occurring in the winter and the minimum occurring in the summer. For the 2015–2019 period, the concentration almost followed a downward trend from January to June except for February. Average concentrations of NO_2 and $PM_{2.5}$ in February 2015–2019 were lower than the expected seasonal levels. This was strongly associated with favorable diffusion weather conditions in February, with higher wind speed (Fig. 2d) and lower relative humidity relative to the adjacent period (Fig. S3).

Although, February 2020 was in the strictest control period, $PM_{2.5}$ concentration was considerably higher than the same period during the preceding five years with a 17 μg/m^3 increase (Fig. 2b), primarily attributed to the extreme stagnant and humid meteorological conditions at the start of the COVID-19 lockdown period (Chang et al., 2020; Le et al., 2020), corresponding to 52% lower boundary layer height (Figs. 2c), 24% lower wind speed (Figs. 2d) and 29% higher relative humidity (Fig. S3) as compared to the average level in other periods. The frequent southern winds also transported air pollution from the south of Beijing (Fig. S3). The reductions in NO_2 and $PM_{2.5}$ concentrations caused by the lockdowns were probably offset by meteorological impacts, especially for $PM_{2.5}$. A clear difference for meteorology between April and May in 2020 was observed with favorable diffusion conditions in April and relatively poor diffusion conditions in May (Fig. 2c and d). Although the observed $PM_{2.5}$ concentrations in April 2020 were lower than that of May, the levels in April could be primarily attributed to emissions changes, while the levels in May were mainly associated with meteorological impacts.

3.1.2. Diurnal variations

The diurnal variations of average NO_2 (a) and $PM_{2.5}$ (b) concentrations using all measurements at GC by Pre-LD, LD and Post-LD are shown in Fig. 3. There were large differences in pollutant concentrations between different periods with the highest level in Pre-LD and the lowest level in Post-LD. The patterns were caused by the combination of weather conditions, seasonal changes, and atmospheric chemistry (Silver et al., 2020; Singh et al., 2020).

For the diurnal variations of NO_2, it presented the characteristic of reaching a minimum during the day and a maximum at night (Fig. 3a). NO_2 retains high and stable levels at night due to equilibrium chemical reactions (Richards, 1983) and stable boundary layer heights, then as the sun rises, NO_2 is rapidly destroyed by photochemical reactions and the boundary layer heights promote the dispersion of pollutants (Chu et al., 2019; Wang et al., 2020a). The highest level occurred at 11pm-8am with means of 54 μg/m^3 and 28 μg/m^3 for Pre-LD and LD, respectively. The highest concentration occurred at 11pm-6am with a mean of 34 μg/m^3 for Post-LD. NO_2 concentration declined earlier during Post-LD, which was mainly due to the earlier sunrise time in the summer than the winter. The concentrations kept dropping until 2–5pm when they reached the lowest level with means of 29 μg/m^3, 16 μg/m^3 and 12 μg/m^3 for Pre-LD, LD, and Post-LD, respectively.

Due to the diurnal variation of the heights of the boundary layer, the $PM_{2.5}$ diurnal patterns (Fig. 3b) also presented the characteristics of an afternoon minimum during the day and a maximum occurring at night (Manning et al., 2018). The difference was that there was a small peak for $PM_{2.5}$ during the day, while no clear peak for NO_2, which probably related to different chemical reaction processes for $PM_{2.5}$ and NO_2. NO_2 is destroyed by active photochemical reactions during the day, while vigorous new particle formation due to increased precursor emissions and atmospheric oxidation during the day (Zhou et al., 2020). For Pre-LD and Post-LD, the daytime peak of $PM_{2.5}$ occurred from about 8am to 2pm with means of 64 μg/m^3 and 39 μg/m^3, respectively. During LD, there was a delayed increase from 10am to 5pm with a mean concentration of 60 μg/m^3.

3.2. Evaluation of the GAM analysis

The meteorological variables input for the GAM for 34 sites are shown in Table S4. The 3-hr rolling average of ERA5 BLH was included for all sites. Sensitivity analysis was used to detect the optimal data source from ERA5, ISD, and BJ for hourly wind factors. The winds from ISD were the optimal choice for most sites, with exception that ERA5 was used at the sites located mostly in the rural area. This was because the ground meteorology observation stations are usually concentrated in the urban area, far away from the air quality monitoring sites in the rural areas. An approximation to the local weather conditions for rural sites can be obtained from the interpolated high resolution ERA5 dataset. For additional optimal variables, the ERA5 D2M, BJ RH, and BJ T2M were

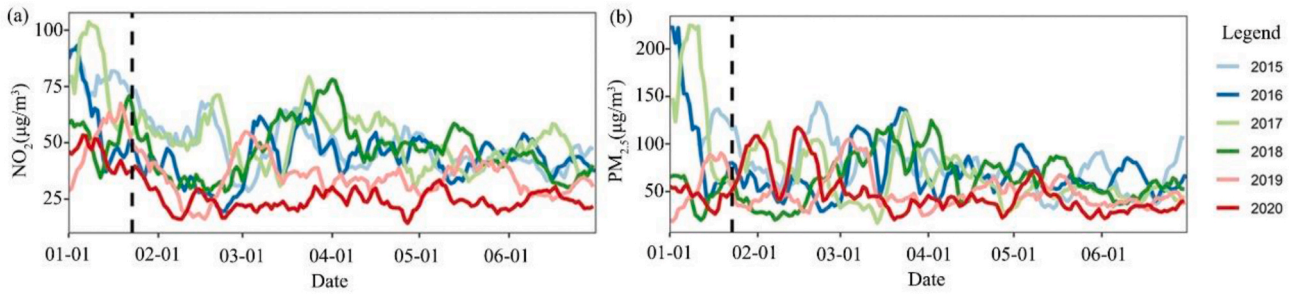

Fig. 1. The time series of preceding 10 days rolling average concentration of NO_2 (a) and $PM_{2.5}$ (b) in each year.

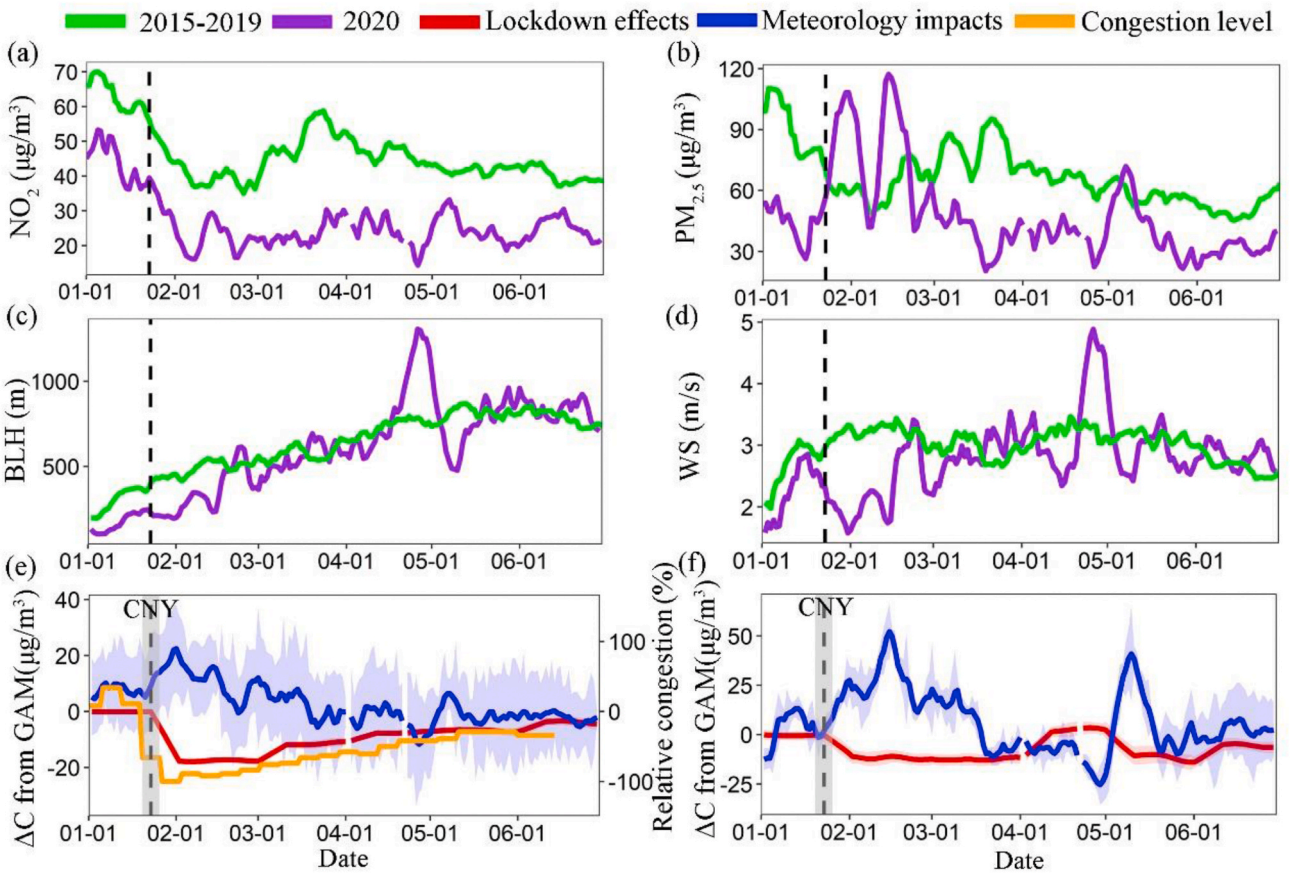

Fig. 2. First two panels: time series of preceding 10 days rolling average observed concentrations of NO_2 (a) and $PM_{2.5}$ (b) and the meteorological observations for boundary layer height (c) and wind speed (d) grouped by 2015–2019 (green lines) and 2020 (purple lines) using all data points. Bottom: time series of preceding 10 days rolling average with the concentration changes due to the lockdowns (red lines) and local meteorological factors (blue lines) estimated from GAM analysis for NO_2 (e) and $PM_{2.5}$ (f) at GC. The orange lines represent the relative congestion level in 2020 compared to 2019. The shaded region represents the standard deviation of pollutant concentrations. The black dotted lines represent the first day of COVID-19 lockdown (January 23, 2020). The gray background represents the Chinese New Year (CNY) and Second Wave (SW) of COVID-19 in Beijing. (For interpretation of the references to colour in this figure legend, the reader is referred to the Web version of this article.)

the most frequent variables used in the NO_2 models, whereas ISD D2M, BJ RH, BJ T2M, and BJ P were frequently included in the $PM_{2.5}$ models.

After accounting for the optimal variables' selection and excluding outliers based on the Iteratively Reweighted Least Squares method for the model of each site, r^2 was in a range of 0.51–0.71 for NO_2 and a range of 0.57–0.63 for $PM_{2.5}$ depending on the sites (Table S1). The square root of the variance of the residuals (RMSE) varied from 0.16 μg/m^3 to 0.54 μg/m^3 for NO_2 models and from 0.52 μg/m^3 to 0.67 μg/m^3 for $PM_{2.5}$ models. The model can explain about 60% of the variance of NO_2 and $PM_{2.5}$ concentrations. The limit of model performance is determined by the uncertainty in the meteorology dataset, for example uncertainties in the simulation of the boundary layer height. The r^2 was somewhat lower and RMSE was somewhat higher for the hourly models than for the daily models (Hua et al., 2021b) mainly due to the high variability of hourly measurements and the greater difficulty in simulating the diurnal profiles. The lower model performance for the sites located in rural areas relative to the sites located in downtown and suburban can be seen in Table S1. This is probably mainly due to the sparse ground meteorological observation stations (Fig. S1). Although the interpolated ERA5 was used to try to approximate the local weather conditions, model simulations still have higher uncertainty than ground-based observations. The residuals from model results for NO_2 (Fig. S4) and $PM_{2.5}$ (Fig. S5) are normally distributed, taking GC as an example.

To estimate the uncertainty of the lockdown scaling factors obtained from the GAM analysis, the standard deviations were calculated from 100 bootstrapping realizations (Table S5). For the scaling factors of NO_2, the average standard deviation was 8% for FEB, 6.6% for MAR, 6.2% for APR, 7.8% for MAY, and 7% for JUN. The standard deviations of $PM_{2.5}$ factors were around 16.5% for FEB, 14.9% for MAR, 15.2% for APR, 18.9% for MAY, and 15.6% for JUN. The uncertainty for $PM_{2.5}$ was somewhat larger than for NO_2, mainly because $PM_{2.5}$ is influenced by complex factors such as transport, various emission sources, and day to day carry over, while NO_2 is mostly influenced by local emissions (Khuzestani et al., 2018; (Zhang et al., 2016b); Liu et al., 2019). The uncertainty expressed by differences in concentrations for each period as shown in Fig. S6 presents the probability density distribution of NO_2 concentration changes at GC. The standard deviations for difference in NO_2 concentrations are about 8 μg/m^3 for FEB and MAR, 5 μg/m^3 for APR to JUN, and 2 μg/m^3 for Pre-LD. The uncertainty in $PM_{2.5}$ concentrations are about 13 μg/m^3 for FEB, MAR, and MAY, 10 μg/m^3 for APR and JUN, and 5 μg/m^3 for Pre-LD. The relatively higher uncertainty for FEB to JUN than Pre-LD might be because there are fewer data points.

The changes of r^2 and RMSE were stable between sites and the changes of uncertainty were stable with the change of site and time suggesting that the model results were robust. The probability density functions of the concentration changes in Fig. S6 show that there are robust differences between the monthly factors. The effects estimated during each period were consistent across most bootstrapped simulations and were not influenced by extreme conditions.

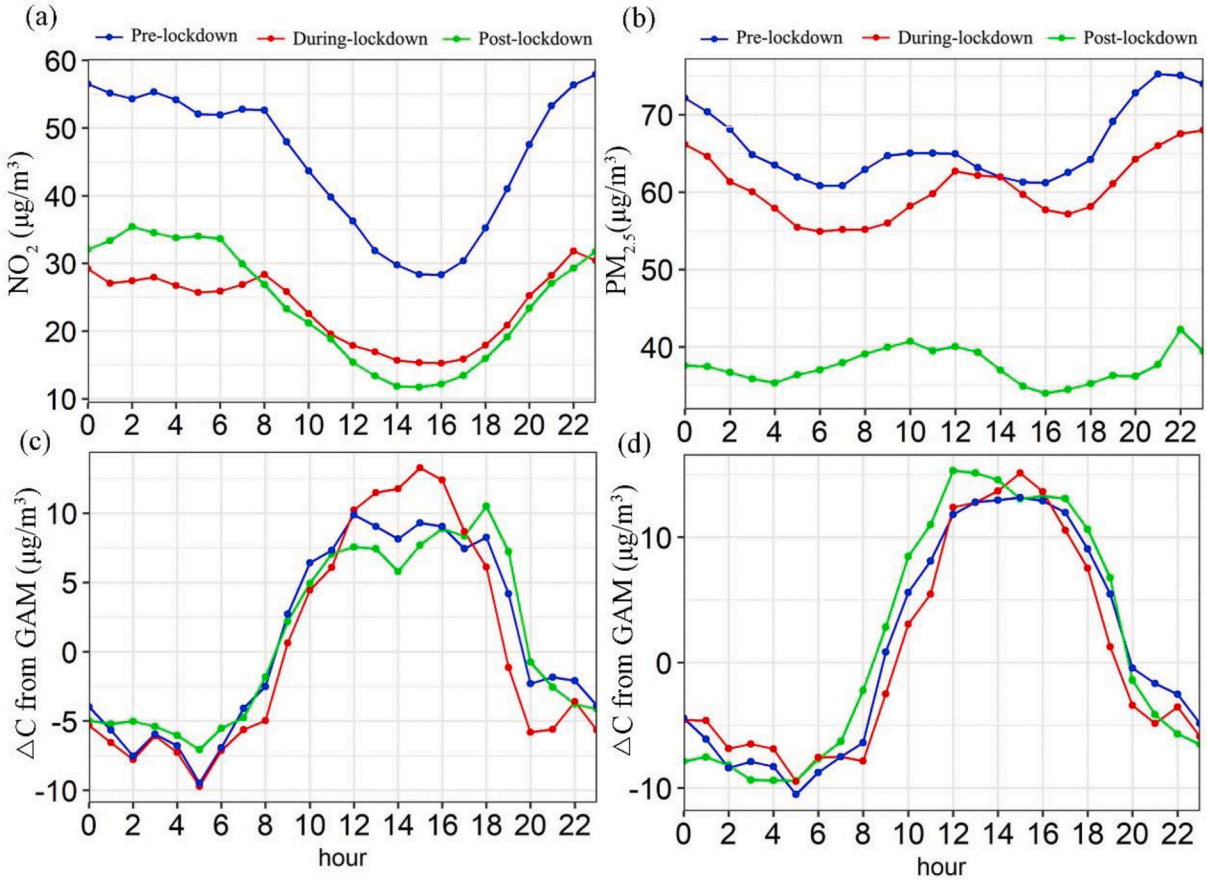

Fig. 3. Top: diurnal variations in averaged measured concentrations of NO_2 (a) and $PM_{2.5}$ (b) for the pre-lockdown, during lockdown and post-lockdown periods at GC. Bottom: changes in concentrations based on GAM analysis of NO_2 (c) and $PM_{2.5}$ (d) for the pre-lockdown, during lockdown and post-lockdown periods at GC.

3.3. Separated meteorology and lockdown effects

The GAM analysis provides a Percent Relative Effect (Eq. (2)) of each factor in the analysis, including both temporal and meteorological impacts. These were averaged monthly to estimate the contributions of meteorology and the lockdown to the variability in NO_2 and $PM_{2.5}$ (Fig. 4). The Percent Relative Effect represents the percentage changes of pollutant concentrations relative to the baseline in the GAM simulation over the entire measurement time period. The seasonal factor includes the monthly factors, as well as the factors for temperature and relative humidity which covary with the seasons, because the relative humidity plays the most important role in air quality among the three factors. The seasonal factors are therefore mostly related to humid weather conditions. As reported in a related study (Hua et al., 2021b), the opposite holiday effects of NO_2 and $PM_{2.5}$ were also observed. The interannual trends suggested that long-term control policies contributed to reductions of 26% for NO_2 and 46% for $PM_{2.5}$ from 2015 to 2020 during January to June. Frequent strong cold local horizonal winds during the winter contribute to disperse pollutant and the breeze horizonal winds during the summer contribute to increase of concentrations. Favorable vertical dispersion frequently occur in the summer and unfavorable vertical dispersion frequently occur in the winter. BLH and seasonal factors had the largest contributions to pollutant concentration increases in January and February. In particular, lower vertical mixing favored increased NO_2 concentrations and more humid conditions favored reduced $PM_{2.5}$. In February, the lockdown measures caused large reductions while meteorology offset a lot of the decrease in surface concentrations. BLH caused 17% increase of NO_2 and humid conditions caused 64% increase of $PM_{2.5}$ relative to the baseline level.

The lockdown effects of NO_2 showed a clear pattern with the strongest reduction in FEB and gradually increased emissions until JUN. This corresponds to NO_2 reductions of 19 $\mu g/m^3$ in FEB, 13 $\mu g/m^3$ in MAR, 9 $\mu g/m^3$ in APR, 8 $\mu g/m^3$ in MAY and 5 $\mu g/m^3$ in JUN (Fig. 2e). The patterns were consistent with the relative congestion level in 2020 compared to 2019, which can be used as a reference to reflect traffic volumes. There are limitations to using TomTom Data to represent the traffic in Beijing because it is not as popular for vehicle navigation systems or cell phone maps as AutoNavi. For the lockdown effect of $PM_{2.5}$, the concentration declined by 12 $\mu g/m^3$ in FEB, 12 $\mu g/m^3$ in MAR, 11 $\mu g/m^3$ in MAY, 6 $\mu g/m^3$ in JUN, while it rebounded in APR with value of 1 $\mu g/m^3$ higher than normal levels (Fig. 2f). The temporal variation of $PM_{2.5}$ was consistent with the study of the Centre for Research on Energy and Clean Air (2020b) which found that $PM_{2.5}$ levels over China clearly rebounded in April and had a 15% reduction in May and June in 2020 compared to the previous year after normalizing for weather. The reason that $PM_{2.5}$ rebounded in APR might be attributed to the recovery of industrial production which caused a large increase in coal consumption. The outputs of cement and metals were 4% higher in April 2020 compared with the previous year, whereas they were 18% lower in March, implying a fast recovery of high emissions industries in China (Centre for Research on Energy and Clean Air, 2020a). There was less of a decline for $PM_{2.5}$ than NO_2 in the start of the lockdown period mainly due to different emission sources, NO_2 emissions are dominated by transportation activities while $PM_{2.5}$ has a strong relationship with residential coal burning and industrial activities, which were less influenced by the lockdowns (Diamond and Wood, 2020). Especially in the heating season, reduced outdoor activities during the lockdown period probably led to an increase in indoor coal burning for heating activities (Hua et al., 2021b).

Unfavorable weather had a large contribution in air pollution in FEB

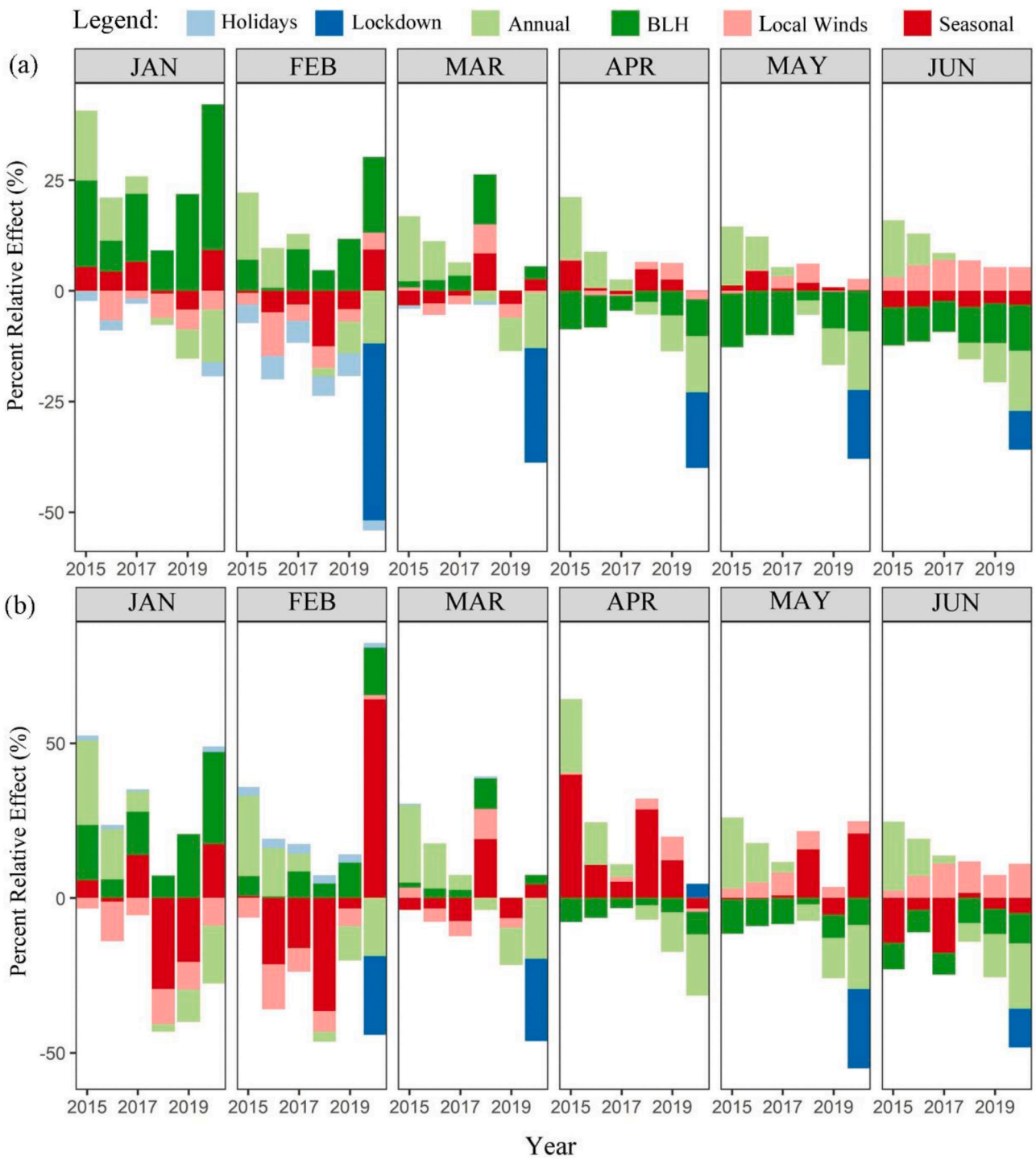

Fig. 4. The Percent Relative Effect of holidays, lockdown, annual, BLH, local wind components and seasonal factors on NO_2 (a) and $PM_{2.5}$ (b) concentrations. The seasonal factor includes monthly variation and the combined influence of RH, T2M, D2M and SP. The holiday and lockdown effects represent the percentage changes of pollutant concentrations relative to the non-holidays and non-lockdowns, the effects of other factors represent the percentage changes of pollutant concentrations during the time interval relative to long-term trends.

and the meteorological conditions in MAY contributed to higher $PM_{2.5}$ concentrations than in APR. The contributions of meteorology to NO_2 and $PM_{2.5}$ show consistent variation. The GAM analysis estimates that meteorology contributed to NO_2 changes of about 12 μg/m^3 in FEB, 3 μg/m^3 in MAR, −3 μg/m^3 in APR, −1 μg/m^3 in MAY, and −2 μg/m^3 in JUN (Fig. 2e). For $PM_{2.5}$, meteorological factors had a pronounced influence with a contribution of about 30 μg/m^3 in FEB, 7 μg/m^3 in MAR, −13 μg/m^3 in APR, 10 μg/m^3 in MAY, and 2 μg/m^3 in JUN (Fig. 2f). The contribution of meteorology was larger than expected in January compared to baseline and long-term trend.

3.4. Spatial-temporal patterns of the lockdown effects

3.4.1. Monthly changes

Fig. 5 presents the spatial patterns of NO_2 percentage changes for 34 sites from FEB to JUN relative to Pre-LD based on GAM analysis. The sites close to the industrial area went back to normal fast, for example, TZ, YF, YLD, and YG average NO_2 concentrations increased by about

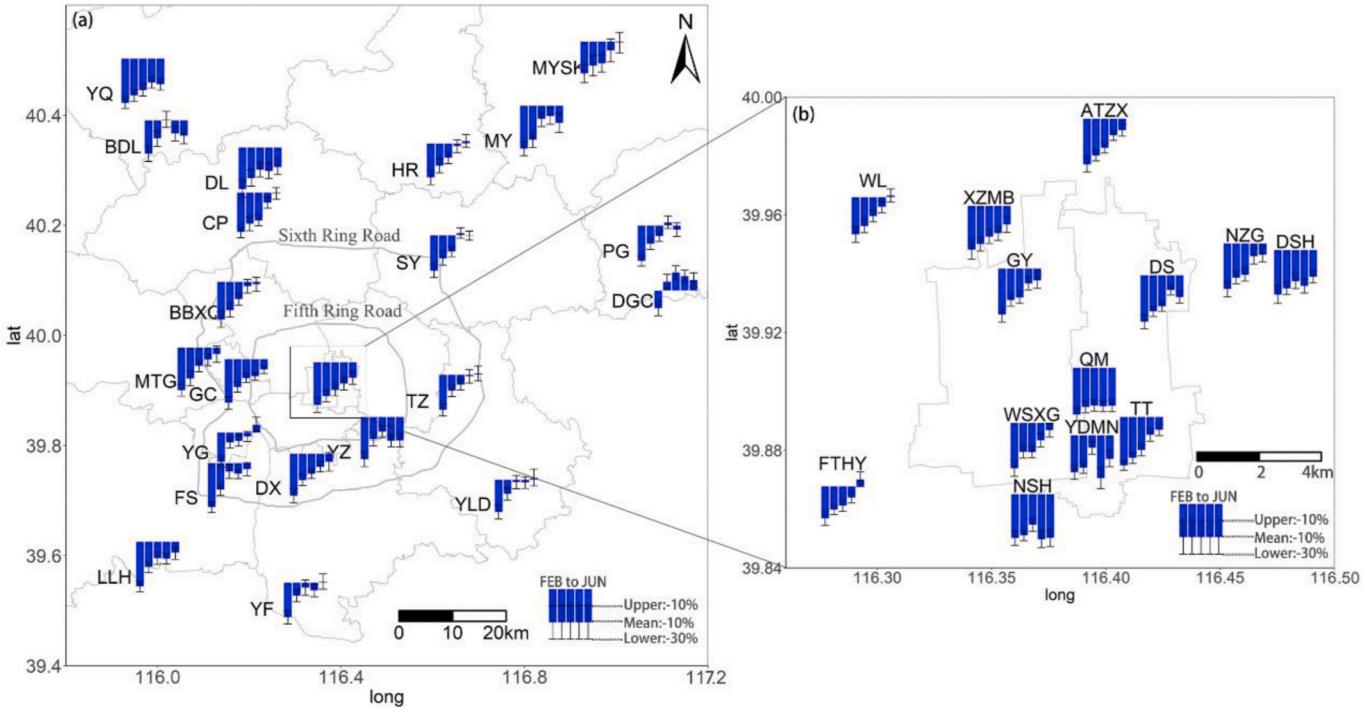

Fig. 5. Time-varying percentage changes of NO_2 concentrations for 34 sites from FEB to JUN relative to Pre-LD based on scaling factors from GAM analysis. (a): The sites outside of Fifth Ring Road. (b): The sites within Fifth Ring Road. The subplot within the black rectangle represents mean lockdown effects of the sites within Fifth Ring Road. The blue bars represent mean percentage changes in NO_2 concentrations. The upper and lower error bars represent the uncertainty of lockdown effects obtained from 100 bootstrap runs. All bars have the same scales. (For interpretation of the references to colour in this figure legend, the reader is referred to the Web version of this article.)

22% in MAR than in FEB and almost returned to the expected level in APR (Table S6). This was attributed to the economic recovery over China (Xinhua News Agency, 2020). DSH, NSH, QM, XZMB and YDMN are sites that typically experience busy traffic. These had not yet returned to the expected level by JUN. This was likely due to reduction in the willingness of people to travel even after the COVID-19 epidemic was brought under control.

The strength of NO_2 reductions was strongly associated with urbanization. Downtown areas show the largest reduction in NO_2 concentrations for MAR, APR, MAY, and JUN with reductions that were about 2%, 9%, 8%, and 8% larger than the suburban sites and about 4%, 11%, 11%, and 7% larger than at the rural sites (Table 2). In FEB, NO_2 concentration for the downtown area was 6% higher than the suburban area and 4% higher than the rural area. The possible reason for this was that the strict COVID-19 control measures resulted in a sharp initial drop in the traffic volume of heavy-duty diesel vehicles, which were normally only allowed to pass in the outside of the Fifth Ring Road (Yang et al., 2015; Wang et al., 2020d). Chinese New Year coincided with the lockdowns, even though the holiday effect was separated from the lockdown effect in this study, millions of commuters returned to their hometown before Chinese New Year, and public transportation suspensions in FEB resulted in sharply drop in traffic volumes in the suburban area (Zhao et al., 2020; Chen et al., 2019).

The spatial pattern of $PM_{2.5}$ lockdown effects (Fig. 6) show that the largest rebound of $PM_{2.5}$ concentration in APR occurred at YLD and TZ, the sites closest to manufacturing factories with higher concentrations than normal, 49% and 44%, respectively. The rebounding of $PM_{2.5}$ in APR at the rural, suburban, and downtown areas gradually weakened, corresponding to 44%, 40%, and 34% increases from MAR. This consistent rebound over all sites suggests that $PM_{2.5}$ concentrations are strongly related to regional emissions. For a few downtown sites (e.g. ATZX, DS, DSH, NZG, QM, TT, YDMN), which experienced approximately 60% reductions in FEB and MAR, the concentrations had not reached the normal level even after a rebound.

The overall strength of $PM_{2.5}$ changes from FEB to JUN shows that the largest reduction was in downtown areas and the lowest reduction was in suburban areas. $PM_{2.5}$ was majorly influenced by industrial and residential emissions, which usually existed in the outside of Fifth Ring Road, and less influenced by control measures (Hua et al., 2021b; Zhi et al., 2017; Cai et al., 2018; Zhang et al., 2008).

3.4.2. *Diurnal profiles*

The diurnal profiles from the GAM analysis can separate the impacts from meteorology and temporal changes on concentrations of NO_2 and $PM_{2.5}$. By accounting for vertical mixing and horizontal dispersion the diurnal profile from the GAM analysis approximate the diurnal profile of estimated emissions (Fig. 3c and d). Although meteorology has different effects on NO_2 and $PM_{2.5}$, the GAM diurnal profiles show similar

Table 2
Time-varying lockdown effects of NO_2 and $PM_{2.5}$ concentrations at the downtown, suburban and rural areas based on the scaling factors from GAM analysis. Scaling factors represent the percentage changes of concentrations in a certain period relative to the Pre-LD period.

Region	NO_2					$PM_{2.5}$				
	FEB (%)	MAR (%)	APR (%)	MAY (%)	JUN (%)	FEB (%)	MAR (%)	APR (%)	MAY (%)	JUN (%)
Downtown	−39	−29	−23	−15	−11	−47	−51	−16	−30	1
Suburban	−45	−27	−14	−7	−3	−28	−24	16	−26	4
Rural	−43	−25	−12	−4	−4	−32	−30	14	−26	−8

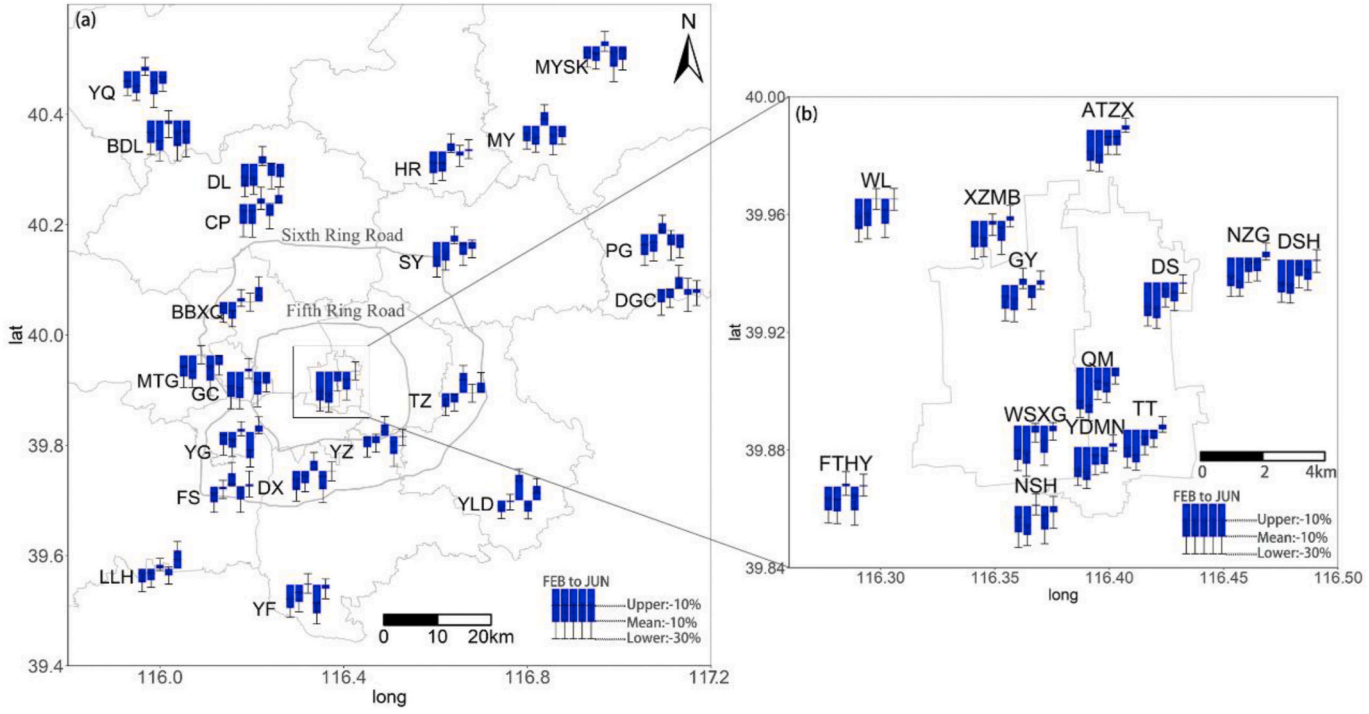

Fig. 6. Time-varying percentage changes of $PM_{2.5}$ concentrations for 34 sites from FEB to JUN relative to Pre-LD based on scaling factors from GAM analysis. (a): The sites outside of Fifth Ring Road. (b): The sites within Fifth Ring Road. The subplot within the black rectangle represents mean lockdown effects of the sites within Fifth Ring Road. The blue bars represent mean percentage changes in $PM_{2.5}$ concentrations. The upper and lower error bars represent the uncertainty of lockdown effects obtained from 100 bootstrap runs. All bars have the same scales. (For interpretation of the references to colour in this figure legend, the reader is referred to the Web version of this article.)

patterns. The diurnal changes of NO_2 concentrations from GAM analysis (Eq. (3)) were grouped to Pre-LD, LD, and Post-LD. For both Pre-LD and Post-LD periods, NO_2 concentrations at GC show a substantial increase from 5am to 10am, being 14 μg/m^3 higher than baseline conditions and a sharp decline from 6pm to 8pm, with levels 11 μg/m^3 lower than the 24-hr average (Fig. 3c). These changes related to increased traffic volumes during the early morning, and decreased traffic at night (Jing et al., 2016). During LD, the morning increase was more gradual and the afternoon decrease occurred sooner. A small daytime peak occurred from 12pm to 5pm, with an average of 11 μg/m^3 NO_2 concentrations higher than the baseline (Fig. 3c). (Huang et al., 2020) reported that the secondary aerosol reached the minimum level from 12pm to 5pm in the day-time during the lockdowns, therefore, the peak was probably because of the increased traffic volumes due to people going outside for necessities. Two small travel peaks were observed from 1 to 4pm and 8–10pm during Pre-LD, NO_2 emissions in LD and Post-LD were both lower than the same period in Pre-LD, this could be due to the impacts of the COVID-19 pandemic, resulting in reduced entertainment activities (China Urban Transportation Report, 2020). For diurnal variation in $PM_{2.5}$ concentration changes, it demonstrates a similar travel peak in the early afternoon during LD, with a 13 μg/m^3 increase relative to the 24-hr average (Fig. 3d).

The spatial patterns of NO_2 (Fig. S7) and $PM_{2.5}$ (Fig. S8) diurnal variations in adjusted concentrations (Eq. (4)) for 34 sites based on GAM analysis were similar with emissions increased during the daytime and declined at night. The travel peak at about 12pm–5pm during LD was more pronounced in the suburban area. In downtown, the sites (e.g. DS, FTHY, NZG, WSXG) mainly of residential areas, and demonstrated a travel peak in LD, whereas the sites close to major ring roads (e.g. DSH, NSH, QM) had lower NO_2 emissions during LD than the same period during Pre-LD, reflecting that people preferred to travel only short distances for necessities during the strictest lockdown period (China Urban Transportation Report, 2020). There were more variations for the diurnal changes at rural sites. BDL and DGC show different patterns as they are located in forested areas and are far away from built-up areas. Consequently, they are less influenced by human activities (Fig. S7).

4. Conclusions

GAM was developed based on hourly measurements of NO_2 and $PM_{2.5}$ from 34 sites in Beijing, China, from January to June in 2015–2020 to quantitatively identify the effects of the COVID-19 lockdown measures and meteorological impacts on air quality. The measurements showed that Beijing experienced extreme haze episodes at the start of the lockdown along with unfavorable weather conditions. The COVID-19 lockdown effects and diurnal changes from the models were not consistent with the measured trends, suggesting that meteorology had a significant impact on pollutant concentrations. During the COVID-19 lockdown period, control measures led to 19 μg/m^3 reductions in NO_2 and 12 μg/m^3 reductions in $PM_{2.5}$, whereas meteorology contributed about 12 μg/m^3 increase in NO_2 and larger in $PM_{2.5}$ with about 30 μg/m^3 increase. Among meteorological factors, BLH caused 17% increase in NO_2 and humid conditions caused 64% increase in $PM_{2.5}$ relative to the baseline level. The results of this study show that air pollution control strategies need to be implemented at different levels according to different weather conditions. The effects on NO_2 and $PM_{2.5}$ due to the COVID-19 lockdown varied with time and depending on the sites, it is necessary to implement key managements for hotspot emission areas.

The GAM method developed in this study can provide a more quantitative estimate of air quality changes caused by control measures, and it can be used for the evaluation of long-term control such as Action Plan on Prevention and Control of Air Pollution and temporary control measures such as APEC Blue impacts on air quality, thereby contributing to the formulation of Beijing's air pollution control policies.

Declaration of competing interest

The authors declare that they have no known competing financial interests or personal relationships that could have appeared to influence the work reported in this paper.

Acknowledgements

This work was supported by the National Natural Science Foundation of China (NSFC, No. 41877310), partly by the National Key Research and Development Program of China (No. 2016YFC0503600) and the Major Science and Technology Projects of Qinghai Province in 2018 (2018-SF-A4). We would like to thank Sophia Wells for providing language help.

Appendix A. Supplementary data

Supplementary data to this article can be found online at https://doi.org/10.1016/j.jenvman.2021.112676.

CRediT author contribution statement

Jinxi Hua: Conceptualization, Formal analysis, Visualization, Writing – original draft. Yuanxun Zhang: Supervision, Funding acquisition, Writing – review & editing. Benjamin de Foy: Conceptualization, Formal analysis, Writing – review & editing. Jing Shang: Writing – review & editing. James J. Schauer: Writing – review & editing. Xiaodong Mei: Writing – review & editing. Ishaq Dimeji Sulaymon: Writing – review & editing. Tingting Han: Formal analysis.

References

Bao, R., Zhang, A., 2020. Does lockdown reduce air pollution? Evidence from 44 cities in northern China. Sci. Total Environ. 731, 139052. https://doi.org/10.1016/j.scitotenv.2020.139052.

Baumgartner, J., Clark, S., Carter, E., Lai, A., Zhang, Y., Shan, M., Schauer, J.J., Yang, X., 2019. Effectiveness of a household energy package in improving indoor air quality and reducing personal exposures in rural China. Environ. Sci. Technol. 53 (15), 9306–9316. https://doi.org/10.1021/acs.est.9b02061.

Bauwens, M., Compernolle, S., Stavrakou, T., Müller, J.F., Gent, J., Eskes, H., Levelt, P.F., A, R., Veefkind, J.P., Vlietinck, J., Yu, H., Zehner, C., 2020. Impact of coronavirus outbreak on NO2 pollution assessed using TROPOMI and OMI observations. Geophys. Res. Lett. https://doi.org/10.1029/2020gl087978.

Cai, S., Li, Q., Wang, S., Chen, J., Ding, D., Zhao, B., Yang, D., Hao, J., 2018. Pollutant emissions from residential combustion and reduction strategies estimated via a village-based emission inventory in Beijing. Environ. Pollut. 238, 230–237. https://doi.org/10.1016/j.envpol.2018.03.036.

Centre for Research on, 2020a. Energy and Clean Air. https://energyandcleanair.org/wp/wp-content/uploads/2020/05/China-air-pollution-rebound-final.pdf.

Centre for Research on, 2020b. Energy and Clean Air. https://energyandcleanair.org/tracker/covid-19-air-pollution-rebound-tracker/.

Chang, Y., Huang, R.J., Ge, X., Huang, X., Hu, J., Duan, Y., Zou, Z., Liu, X., Lehmann, M. F., 2020. Puzzling haze events in China during the coronavirus (COVID-19) shutdown. Geophys. Res. Lett. 47 (12), e2020GL088533 https://doi.org/10.1029/2020gl088533.

Chen, P.-Y., Tan, P.-H., Chou, C.C.K., Lin, Y.-S., Chen, W.-N., Shiu, C.-J., 2019. Impacts of holiday characteristics and number of vacation days on "holiday effect" in Taipei: implications on ozone control strategies. Atmos. Environ. 202, 357–369. https://doi.org/10.1016/j.atmosenv.2019.01.029.

China Urban Transportation Report, 2020. http://huiyan.baidu.com/reports/landing?id=63.

Chu, B., Zhang, S., Liu, J., Ma, Q., He, H., 2020. Significant concurrent decrease in PM2.5 and NO2 concentrations in China during COVID-19 epidemic. J. Environ. Sci. 99, 346–353. https://doi.org/10.1016/j.jes.2020.06.031.

Chu, Y., Li, J., Li, C., Tan, W., Su, T., Li, J., 2019. Seasonal and diurnal variability of planetary boundary layer height in Beijing: intercomparison between MPL and WRF results. Atmos. Res. 227, 1–13. https://doi.org/10.1016/j.atmosres.2019.04.017.

Cui, Y., Ji, D., Maenhaut, W., Gao, W., Zhang, R., Wang, Y., 2020. Levels and sources of hourly PM2.5-related elements during the control period of the COVID-19 pandemic at a rural site between Beijing and Tianjin. Sci. Total Environ., 140840 https://doi.org/10.1016/j.scitotenv.2020.140840.

de Foy, B., Schauer, J.J., 2019. Changes in speciated PM2.5 in Fresno, California, due to NOx concentrations reductions and variations in diurnal emission profiles by day of week. Science of the Anthropocene 7, 45. https://doi.org/10.1525/journal.elementa.384.

de Foy, B., 2018. City-level variations in NOx emissions derived from hourly monitoring data in Chicago. Atmos. Environ. 176, 128–139. https://doi.org/10.1016/j.atmosenv.2017.12.028.

de Foy, B., Brune, W.H., Schauer, J.J., 2020. Changes in ozone photochemical regime in Fresno, California from 1994 to 2018 deduced from changes in the weekend effect. Environ. Pollut. 263, 114380. https://doi.org/10.1016/j.envpol.2020.114380.

de Foy, B., Cui, Y.Y., Schauer, J.J., Janssen, M., Turner, J.R., Wiedinmyer, C., 2015b. Estimating sources of elemental and organic carbon and their temporal emission patterns using a least squares inverse model and hourly measurements from the St. Louis–Midwest supersite. Atmos. Chem. Phys. 15, 2405–2427. https://doi.org/10.5194/acp-15-2405-2015.

de Foy, B., Lu, Z., Streets, D.G., 2016. Satellite NO2 retrievals suggest China has exceeded its NOx reduction goals from the twelfth Five-Year Plan. Sci. Rep. 6, 35912. https://doi.org/10.1038/srep35912.

Diamond, M.S., Wood, R., 2020. Limited regional aerosol and cloud microphysical changes despite unprecedented decline in nitrogen oxide pollution during the february 2020 COVID-19 shutdown in China. Geophys. Res. Lett. 47 https://doi.org/10.1029/2020gl088913.

Fan, C., Li, Y., Guang, J., Li, Z., Elnashar, A., Allam, M., de Leeuw, G., 2020. The impact of the control measures during the COVID-19 outbreak on air pollution in China. Rem. Sens. 12, 1613. https://doi.org/10.3390/rs12101613.

Grange, S.K., Carslaw, D.C., 2019. Using meteorological normalisation to detect interventions in air quality time series. Sci. Total Environ. 653, 578–588. https://doi.org/10.1016/j.scitotenv.2018.10.344.

Griffith, S.M., Huang, W.-S., Lin, C.-C., Chen, Y.-C., Chang, K.-E., Lin, T.-H., Wang, S.-H., Lin, N.-H., 2020. Long-range air pollution transport in East Asia during the first week of the COVID-19 lockdown in China. Sci. Total Environ., 140214 https://doi.org/10.1016/j.scitotenv.2020.140214.

Hua, J., Zhang, Y., de Foy, B., Mei, X., Shang, J., Zhang, Y., Sulaymon, I.D., Zhou, D., 2021a. Improved PM2.5 concentration estimates from low-cost sensors using calibration models categorized by relative humidity. Aerosol. Sci. Technol. 1–14. https://doi.org/10.1080/02786826.2021.1873911.

Hua, J., Zhang, Y., de Foy, B., Mei, X., Shang, J., Feng, C., 2021b. Competing PM2.5 and NO2 holiday effects in the Beijing area vary locally due to differences in residential coal burning and traffic patterns. Sci. Total Environ. 750, 141575. https://doi.org/10.1016/j.scitotenv.2020.141575.

Huang, X., Ding, A., Gao, J., Zheng, B., Zhou, D., Qi, X., Tang, R., Ren, C., Nie, W., Chi, X., Wang, J., Xu, Z., Chen, L., Li, Y., Che, F., Pang, N., Wang, H., Tong, D., Qin, W., Cheng, W., Liu, W., Fu, Q., Chai, F., Davis, S.J., Zhang, Q., He, K., 2020. Enhanced secondary pollution offset reduction of primary emissions during COVID-19 lockdown in China. https://doi.org/10.31223/osf.io/hvuzy.

Jing, B., Wu, L., Mao, H., Gong, S., He, J., Zou, C., Song, G., Li, X., Wu, Z., 2016. Development of a vehicle emission inventory with high temporal–spatial resolution based on NRT traffic data and its impact on air pollution in Beijing – Part 1: Development and evaluation of vehicle emission inventory. Atmos. Chem. Phys. 16, 3161–3170. https://doi.org/10.5194/acp-16-3161-2016.

Khuzestani, R.B., Schauer, J.J., Shang, J., Cai, T., Fang, D., Wei, Y., Zhang, L., Zhang, Y., 2018. Source apportionments of PM2.5 organic carbon during the elevated pollution episodes in the Ordos region, Inner Mongolia, China. Environ. Sci. Pollut. Control Ser. 25, 13159–13172. https://doi.org/10.1007/s11356-018-1514-4.

Le, T., Wang, Y., Liu, L., Yang, J., Yung, Y.L., Li, G., Seinfeld, J.H., 2020. Unexpected air pollution with marked emission reductions during the COVID-19 outbreak in China. Science 369 (6504), 702–706. https://doi.org/10.1126/science.abb7431.

Liu, F., Page, A., Strode, S.A., Yoshida, Y., Choi, S., Zheng, B., Lamsal, L.N., Li, C., Krotkov, N.A., Eskes, H., 2020. Abrupt decline in tropospheric nitrogen dioxide over China after the outbreak of COVID-19. Science Advances, eabc2992. https://doi.org/10.1126/sciadv.abc2992.

Liu, Q., Baumgartner, J., Schauer, J.J., 2019. Source apportionment of fine-particle, water-soluble organic nitrogen and its association with the inflammatory potential of lung epithelial cells. Environ. Sci. Technol. 53, 9845–9854. https://doi.org/10.1021/acs.est.9b02523.

Ma, Y., Ma, B., Jiao, H., Zhang, Y., Xin, J., Yu, Z., 2020. An analysis of the effects of weather and air pollution on tropospheric ozone using a generalized additive model in Western China: Lanzhou, Gansu. Atmos. Environ. 224, 117342. https://doi.org/10.1016/j.atmosenv.2020.117342.

Manning, M.I., Martin, R.V., Hasenkopf, C., Flasher, J., Li, C., 2018. Diurnal patterns in global fine particulate matter concentration. Environ. Sci. Technol. Lett. 5, 687–691. https://doi.org/10.1021/acs.estlett.8b00573.

Mehta, S.K., Ratnam, M.V., Sunilkumar, S.V., Rao, D.N., Krishna Murthy, B.V., 2017. Diurnal variability of the atmospheric boundary layer height over a tropical station in the Indian monsoon region. Atmos. Chem. Phys. 17, 531–549. https://doi.org/10.5194/acp-17-531-2017.

Otmani, A., Benchrif, A., Tahri, M., Bounakhla, M., Chakir, E.M., El Bouch, M., Krombi, M., 2020. Impact of covid-19 lockdown on PM10, SO2 and NO2 concentrations in sale city (Morocco). Sci. Total Environ. 735, 139541. https://doi.org/10.1016/j.scitotenv.2020.139541.

Petetin, H., Bowdalo, D., Soret, A., Guevara, M., Jorba, O., Serradell, K., Pérez García-Pando, C., 2020. Meteorology-normalized impact of the COVID-19 lockdown upon NO_2 pollution in Spain. Atmos. Chem. Phys. 20, 11119–11141. https://doi.org/10.5194/acp-20-11119-2020.

Richards, L.W., 1983. Comments on the oxidation of NO2 to nitrate——day and night, 1967 Atmos. Environ. 17, 397–402.

Shang, J., Khuzestani, R.B., Huang, W., An, J., Schauer, J.J., Fang, D., Cai, T., Tian, J., Yang, S., Guo, B., Zhang, Y., 2018. Acute changes in a respiratory inflammation marker in guards following Beijing air pollution controls. Sci. Total Environ. 624, 1539–1549. https://doi.org/10.1016/j.scitotenv.2017.12.109.

Silver, B., He, X., Arnold, S.R., Spracklen, D.V., 2020. The impact of COVID-19 control measures on air quality in China. Environ. Res. Lett. 15, 084021 https://doi.org/10.1088/1748-9326/aba3a2.

Singh, V., Singh, S., Biswal, A., Kesarkar, A.P., Mor, S., Ravindra, K., 2020. Diurnal and temporal changes in air pollution during COVID-19 strict lockdown over different regions of India. Environ. Pollut. 266, 115368. https://doi.org/10.1016/j.envpol.2020.115368.

Sulaymon, I.D., Zhang, Y.X., Hopke, P.K., Zhang, Y., Hua, J., Mei, X., 2021. COVID-19 pandemic in Wuhan: ambient air quality and the relationships between criteria air pollutants and meteorological variables before, during, and after lockdown. Atmos. Res. 250, 105362.

Sun, Y., Lei, L., Zhou, W., Chen, C., He, Y., Sun, J., Li, Z., Xu, W., Wang, Q., Ji, D., Fu, P., Wang, Z., Worsnop, D.R., 2020. A chemical cocktail during the COVID-19 outbreak in Beijing, China: insights from six-year aerosol particle composition measurements during the Chinese New Year holiday. Sci. Total Environ., 140739 https://doi.org/10.1016/j.scitotenv.2020.140739.

Tian, H., Liu, Y., Li, Y., Wu, C.-H., Chen, B., Kraemer, M.U., Li, B., Cai, J., Xu, B., Yang, Q., 2020. An investigation of transmission control measures during the first 50 days of the COVID-19 epidemic in China. Science 368, 638–642.

Tian, J., Cai, T., Shang, J., Schauer, J.J., Yang, S., Zhang, L., Zhang, Y., 2019. Effects of the emergency control measures in Beijing on air quality improvement. Atmospheric Pollution Research 10, 580–586. https://doi.org/10.1016/j.apr.2018.10.005.

Venter, Z.S., Aunan, K., Chowdhury, S., Lelieveld, J., 2020. COVID-19 lockdowns cause global air pollution declines. Proc. Natl. Acad. Sci. U. S. A. 117 (32), 18984–18990. https://doi.org/10.1073/pnas.2006853117.

Wang, H., Li, Z., Lv, Y., Zhang, Y., Xu, H., Guo, J., Goloub, P., 2020a. Determination and climatology of the diurnal cycle of the atmospheric mixing layer height over Beijing 2013–2018: lidar measurements and implications for air pollution. Atmos. Chem. Phys. 20, 8839–8854. https://doi.org/10.5194/acp-20-8839-2020.

Wang, P., Chen, K., Zhu, S., Wang, P., Zhang, H., 2020b. Severe air pollution events not avoided by reduced anthropogenic activities during COVID-19 outbreak. Resour. Conserv. Recycl. 158, 104814. https://doi.org/10.1016/j.resconrec.2020.104814.

Wang, Q., Su, M., 2020c. A preliminary assessment of the impact of COVID-19 on environment - a case study of China. Sci. Total Environ. 728, 138915. https://doi.org/10.1016/j.scitotenv.2020.138915.

Wang, Y., de Foy, B., Schauer, J.J., Olson, M.R., Zhang, Y., Li, Z., Zhang, Y., 2017. Impacts of regional transport on black carbon in Huairou, Beijing, China. Environ. Pollut. 221, 75–84. https://doi.org/10.1016/j.envpol.2016.11.006.

Wang, Y., Wen, Y., Wang, Y., Zhang, S., Zhang, K.M., Zheng, H., Xing, J., Wu, Y., Hao, J., 2020d. Four-month changes in air quality during and after the COVID-19 lockdown in six megacities in China. Environ. Sci. Technol. Lett. 7 (11), 802–808. https://doi.org/10.1021/acs.estlett.0c00605.

Wang, Y., Zhang, Y., Schauer, J.J., de Foy, B., Guo, B., Zhang, Y., 2016. Relative impact of emissions controls and meteorology on air pollution mitigation associated with the Asia-Pacific Economic Cooperation (APEC) conference in Beijing, China. Sci. Total Environ. 571, 1467–1476. https://doi.org/10.1016/j.scitotenv.2016.06.215.

World Health Organization, 2020. Coronavirus (COVID-2019) Data Reports. https://www.who.int/data#reports.

Yang, Z., Wang, H., Shao, Z., Muncrief, R., 2015. Review of Beijing's comprehensive motor vehicle emission control programs, 102 Communications 49, 847129.

Zhang, H., Wang, S., Hao, J., Wang, X., Wang, S., Chai, F., Li, M., 2016a. Air pollution and control action in Beijing. J. Clean. Prod. 112, 1519–1527. https://doi.org/10.1016/j.jclepro.2015.04.092.

Zhang, Y., Huang, W., Cai, T., Fang, D., Wang, Y., Song, J., Hu, M., Zhang, Y., 2016b. Concentrations and chemical compositions of fine particles (PM2.5) during haze and non-haze days in Beijing. Atmos. Res. 174–175, 62–69. https://doi.org/10.1016/j.atmosres.2016.02.003.

Zhang, Y., Schauer, J.J., Zhang, Y., Zeng, L., Wei, Y., Liu, Y., Shao, M., 2008. Characteristics of particulate carbon emissions from real-world Chinese coal combustion. Environ. Sci. Technol. 42, 5068–5073. https://doi.org/10.1021/es7022576.

Zhao, P., Liu, D., Yu, Z., Hu, H., 2020. Long commutes and transport inequity in China's growing megacity: new evidence from Beijing using mobile phone data. Travel Behaviour and Society 20, 248–263. https://doi.org/10.1016/j.tbs.2020.04.007.

Zhi, G., Zhang, Y., Sun, J., Cheng, M., Dang, H., Liu, S., Yang, J., Zhang, Y., Xue, Z., Li, S., Meng, F., 2017. Village energy survey reveals missing rural raw coal in northern China: significance in science and policy. Environ. Pollut. 223, 705–712. https://doi.org/10.1016/j.envpol.2017.02.009.

Zhou, Y., Brunner, D., Hueglin, C., Henne, S., Staehelin, J., 2012. Changes in OMI tropospheric NO2 columns over Europe from 2004 to 2009 and the influence of meteorological variability. Atmos. Environ. 46, 482–495. https://doi.org/10.1016/j.atmosenv.2011.09.024.

Zhou, Y., Dada, L., Liu, Y., Fu, Y., Kangasluoma, J., Chan, T., Yan, C., Chu, B., Daellenbach, K.R., Bianchi, F., Kokkonen, T.V., Liu, Y., Kujansuu, J., Kerminen, V.-M., Petäjä, T., Wang, L., Jiang, J., Kulmala, M., 2020. Variation of size-segregated particle number concentrations in wintertime Beijing. Atmos. Chem. Phys. 20, 1201–1216. https://doi.org/10.5194/acp-20-1201-2020.

Xinhua News Agency, 2020. http://www.gov.cn/xinwen/2020-04/11/content_5501484.htm (accessed 11 April 2020).

http://www.xinhuanet.com/2020-04/29/c_1125924570.htm, 2020–. (Accessed 29 April 2020).